ELSEVIER

Applied Catalysis A: General 216 (2001) 91–101

APPLIED CATALYSIS A: GENERAL

www.elsevier.com/locate/apcata

Tungsten promoted ammonium and potassium ferrierite: deactivation during the skeletal isomerization of linear butenes

Zunilda R. Finelli, Carlos A. Querini, Nora S. Fígoli, Raúl A. Comelli*

Instituto de Investigaciones en Catálisis y Petroquímica-INCAPE (F.I.Q.-U.N.L., CONICET), Santiago del Estero 2654, S3000AOJ-Santa Fe, Argentina

Received 3 October 2000; received in revised form 13 February 2001; accepted 17 February 2001

Abstract

Deactivation of tungsten promoted ferrierite during the skeletal isomerization of 1-butene at 400°C, atmospheric pressure and 0.15 atm 1-butene partial pressure was studied. Both potassium and ammonium ferrierites were impregnated with tungsten species using either tungstic acid or ammonium metatungstate as precursors, reaching loadings between 1.4 and 7.3%. After the tungsten addition on both ferrierite samples, neither the acid strength distribution nor the total acidity corresponding to the unpromoted materials change significantly. The strongest acid sites present on the ammonium ferrierite with and without tungsten and absent on the tungsten promoted potassium ferrierite, are responsible for the side-reactions. Deactivation of tungsten promoted ferrierites shows differences. Ammonium ferrierite with and without tungsten reach similar carbon contents, being larger than the ones obtained on potassium ferrierite with and without tungsten. In all cases, the carbonaceous deposit shows both olefinic and aromatic species, the proportion depending on the samples. Coke on tungsten promoted potassium ferrierite shows mainly an olefinic nature, while the deposit formed on tungsten promoted ammonium ferrierite has a more aromatic character. For the latter samples, the complete coke removal needs higher temperatures. The strength of acid sites determines not only the carbonaceous deposit amount but also its degree of condensation. The low isobutene selectivity at short time-on-stream (TOS) is avoided by starting the 1-butene feed with the catalytic bed at 200°C and then increasing temperature up to 400°C. It can be considered that a strong adsorption of reactant molecules takes place at low temperatures, thus deactivating the strongest acid sites.

Keywords: Skeletal isomerization; Isobutene; Tungsten/ferrierite; Deactivation; Coke nature

1. Introduction

Isobutene, a very desirable material used in the MTBE synthesis and alkylation reactions, demands alternative production routes. In this way, the skeletal isomerization of linear butenes has achieved a considerable practical interest. This reaction takes place on acid catalysts. Modified amorphous materials, such as tungsten oxide promoted alumina, reach high activity and isobutene selectivity [1–3]. Zeolites having suitable acidity and pore size also appear as active and selective materials [4,5]. Some authors consider that pore structure plays a more important role than acidity to improve the isobutene selectivity [6,7]. The most suitable zeolitic materials are the 10-member ring molecular sieves with pore diameters between 4.0 and 5.5 Å [7,8].

Ferrierite [9] having a two-dimensional pore system with 10-member rings intersected by eight-member rings is one of the best materials employed for the

* Corresponding author. Tel.: +54-0342-4528062; fax: +54-342-4531068.
E-mail address: rcomelli@fiqus.unl.edu.ar (R.A. Comelli).

0926-860X/01/$ – see front matter
PII: S0926-860X(01)00545-2

skeletal isomerization of linear butenes. Nevertheless, the isobutene selectivity is low at short time-on-stream (TOS), it improving when a carbonaceous deposit has been formed [10,11]. Seo et al. [12] demonstrated that this deposit suppresses side-reactions, such as dimerization and cracking, thus increasing the isobutene selectivity. The characteristic behavior with TOS has also been related to a pseudo-monomolecular isomerization mechanism involving, as active sites, benzyl carbocations which result from adsorption of coke molecules on the acid sites [13], although it has been objected by other authors [14]. Pore structure, acidity and operating conditions affect the carbonaceous deposits [15]. During the skeletal isomerization of linear butenes on ferrierite, the carbon content reaches levels between 7 and 9% [12,16,17]. The characterization of coke related to the regeneration of ferrierite has been recently reported [18]. The carbonaceous deposit presents both olefinic and aromatic species, their proportion depending on the operating conditions.

According to previous results [19], potassium ferrierite is inactive in the skeletal isomerization of linear butenes while the addition of tungsten species on this material promotes both activity and isobutene production, also achieving good stability. Calcined ammonium ferrierite shows the characteristic catalytic behavior described above, while the addition of tungsten species improves the isobutene yield. Furthermore, the high activity at short TOS can be diminished enhancing the isobutene selectivity, by starting the linear butene feed with the catalytic bed at a low temperature and then increasing it up to the reaction one. Nevertheless, there are no data available related to deactivation and/or coke characterization when the butene reaction takes place on ferrierite promoted with tungsten species.

In this paper, the deactivation processes of tungsten promoted potassium and ammonium ferrierite that take place during the 1-butene isomerization at 400°C, atmospheric pressure and 0.15 atm 1-butene partial pressure are studied, the alkene feed starting at different catalytic bed temperatures. The carbonaceous deposit is characterized by temperature-programmed oxidation (TPO) and diffuse-reflectance infrared spectroscopy (DRIFTS). Characterization by temperature-programmed reduction (TPR) and ammonia temperature-programmed desorption (NH_3-TPD) is also made in order to relate the material properties with the catalytic behavior, the deactivation process and the nature of coke formed.

2. Experimental

Potassium and ammonium ferrierite samples (identified as KF and AF, respectively) were provided by TOSOH, Japan (samples HSZ-720KOA and HSZ-720NHA, respectively). The SiO_2/Al_2O_3 molar ratio was 17.8; AF has Na_2O and K_2O concentrations below 0.05 and 0.10%, respectively. The crystalline structure was characterized by X-ray diffraction using a Rich-Seifert Iso-Debyeflex 2002 diffractometer, the diffraction spectrum range being $0 < 2\theta < 60^\circ$ [19].

KF and AF samples were impregnated with different tungsten loading following the incipient wetness technique, using tungstic acid (*a*) and ammonium metatungstate (*m*) as tungsten precursors. Solutions with the calculated concentration to obtain a given tungsten loading on the solids were prepared. Tungsten loading varied between 1.4 and 7.3%. After impregnation, samples were maintained for 4 h at room temperature, and then dried overnight in an oven at 110°C. Samples were identified as $W_p(c)$/KF and $W_p(c)$/AF, "p" being the tungsten precursor used for impregnation and "*c*" the tungsten loading on the solid, expressed as weight percent referred to the dried base.

The surface species reducibility was determined by TPR using an Ohkura TP 2002S equipped with a thermal conductivity detector. KF and AF were pretreated in situ in a nitrogen stream (60 ml min^{-1}) heating at 17.5°C min^{-1} and holding 30 min at 550°C; tungsten containing samples were heated at 9.6°C min^{-1} and held 30 min at 600°C, in a nitrogen (60 ml min^{-1}) plus air (50 ml min^{-1}) stream. Then, samples were cooled to room temperature in an argon stream, and finally heated at 10°C min^{-1} up to 950°C in a 1.8% hydrogen in argon stream.

NH_3-TPD measurements were carried out to characterize the total acidity and the acid strength distribution of the catalysts. Samples were pretreated in situ under the same conditions mentioned above. Then, samples were cooled in a nitrogen stream. Ammonia was fed over the bed at 100°C, followed by a purge with nitrogen at 200°C during 120 min. Finally, temperature was raised at 10°C min^{-1} in a nitrogen stream. The ammonia desorption was

continuously measured using a thermal conductivity detector.

The catalytic behavior during the 1-butene skeletal isomerization was measured in a continuous down-flow, fixed-bed quartz tubular reactor operated at the atmospheric pressure, using 500 mg of catalyst sieved to 35–80 mesh. Samples were pretreated in situ under the same previous conditions. After heating, samples were cooled to the desired temperature in a nitrogen stream. For reaction, a pure 1-butene stream was co-fed with nitrogen at 0.15 atm 1-butene partial pressure. Two types of experiments were made: (i) feeding the 1-butene with the catalyst bed at 400°C; (ii) starting the alkene feed with the bed at 200°C and then increasing temperature up to 400°C. The reactant and reaction products were analyzed by on-line gas chromatography, using a 30 m long, 0.54 mm o.d. GS-Alumina (J&W) megabore column, operated isothermally at 100°C. From these data, catalytic activity, selectivity to isobutene, and isobutene yield were calculated on a carbon basis. The catalytic activity is expressed as *n*-butene conversion, grouping together the three linear butene isomers. It is based on the fact that, under reaction conditions, the isomerization of 1-butene to 2-butenes reaches quickly the equilibrium via double-bond migration.

The TPO analysis of used catalysts was performed in an apparatus designed to improve both sensitivity and resolution [20]. Combustion products were completely converted to methane on a nickel catalyst, methane being continuously analyzed by a flame ionization detector. Experiments were carried out using a 6% oxygen in nitrogen stream (20 ml min^{-1}), heating at 12°C min^{-1}. The sample weight was about 0.01 g. Calibration was periodically checked to verify the total conversion of both carbon monoxide and carbon dioxide into methane.

The carbonaceous deposit formed on catalysts was also characterized by DRIFTS using a Shimadzu 8101M spectrometer. Coked samples were powdered and diluted to 5% in potassium bromide.

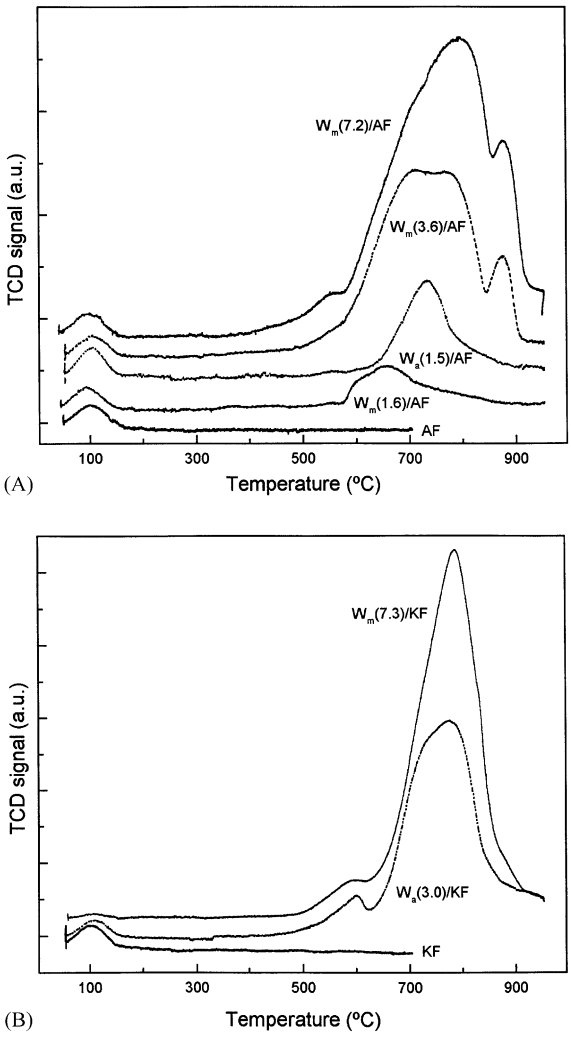

Fig. 1. TPR profiles of different samples. (A): AF with and without tungsten; (B): KF with and without tungsten.

3. Results

Fig. 1A and B present TPR profiles of samples with and without tungsten. AF and KF do not display reduction peak. For W/AF prepared using the "m" precursor, the main reduction peak is broad (could be considered as two overlapped peaks). By increasing the tungsten loading, reduction begins at a lower temperature and the maximum of the main peak shifts to a higher temperature. Above 3.6% tungsten loading another well-defined peak overlapped to the end of the main one appears, while W(7.2)/AF also shows a shoulder at the beginning of the main reduction peak. Comparing at the same tungsten loading, a sharper and more symmetric reduction peak (with its maximum

shifted to a higher temperature) is observed when the "a" precursor is used. W/KF profiles show the main reduction peak (sharper compared to the same tungsten loading on AF) centered at about 780°C and another small peak below 600°C. Differences in the TPR profiles corresponding to the different samples can be related to the tungsten precursor used. The more symmetric peaks obtained using the "a" precursor can be understood considering a better distribution of surface species, while the larger oxoanion size of the "m" precursor would hinder its diffusion into the pores, resulting in a non-uniform distribution and thus giving broader peaks. Tungsten addition on AF and KF generates species, which reduce at high temperature. Then, the tungsten species are not reduced under reaction conditions, still in the presence of 1-butene considered as a reduction medium [21].

NH_3-TPD profiles of different samples are shown in Fig. 2A and B. Calcined AF with and without tungsten display two defined peaks (centered at about 300 and 600°C), assigned to weak and strong acid sites, respectively. It qualitatively agrees with results previously reported [10,12]. KF with and without tungsten only present the peak corresponding to weak acid sites, its maximum being centered at about 340°C. Tungsten addition on AF and KF does not significantly modify the acid strength distribution of the corresponding material without tungsten. Total acidity remains practically constant, only showing a slight decrease for the largest tungsten loading.

Table 1 shows catalytic activity and isobutene yield at 5 and 40 min at 400°C, for samples with and without tungsten and starting the 1-butene feed at different catalyst bed temperature. KF is inactive for the skeletal isomerization. When feeding the 1-butene with the bed at 400°C, AF presents a high catalytic activity with a low isobutene selectivity at short TOS, improving this selectivity with TOS. This behavior has been reported as characteristic of ferrierite [10,22]. When starting the alkene feed with the bed at 200°C and then increasing temperature up to 400°C, the activity at short TOS significantly decreases and the isobutene selectivity improves. Tungsten addition on AF does not qualitatively change the catalytic behavior but produces a synergetic effect over both activity and isobutene production; the best performance is obtained with a 1.5–1.6% tungsten loading. The isobutene selectivity is slightly higher using the "a" precursor, though the isobutene production is similar for both precursors. Tungsten addition on KF promotes both activity and isobutene production, the 3% tungsten loading achieving the best performance. The "a" precursor yields slightly higher activity and isobutene production.

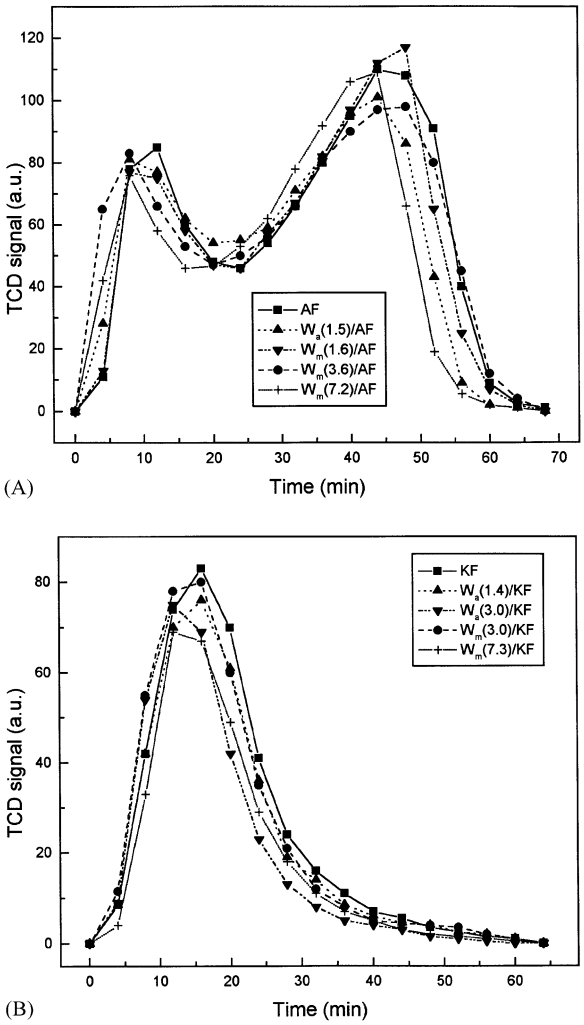

Fig. 2. NH_3-TPD profiles of different samples. (A): AF with and without tungsten; (B): KF with and without tungsten.

The amount of carbonaceous deposit formed after reaction at 400°C during 180 min is shown in Table 1 and Fig. 3. Carbon contents between 6.6 and 8.6% are reached on AF with and without tungsten; it agrees

Table 1
Catalytic activity (expressed as linear butenes conversion, $X_{n\text{-C4=}}$) and isobutene yield ($Y_{i\text{-C4=}}$) at 5 and 40 min at 400°C, and carbon content (%C) after 180 min at 400°C[a]

Sample	T	$X_{n\text{-C4=}}$ (%)		$Y_{i\text{-C4=}}$ (%)		% C
	(°C)	5 min	40 min	5 min	40 min	
KF	400	0.8	0.7	0.2	0.2	0.1
	↑Tr	0.2	0.2	0.1	0.1	0.2
AF	400	69.1	17.6	20.5	11.8	8.3
	↑Tr	16.3	11.5	10.9	9.1	8.6
W_a(1.5)/AF	400	84.0	40.9	19.4	22.1	n.a.
	↑Tr	24.7	22.1	19.0	19.1	7.6
W_m(1.6)/AF	400	84.4	41.9	17.2	21.5	6.8
	↑Tr	35.1	31.3	20.6	20.5	7.7
W_m(3.6)/AF	400	82.6	35.6	16.0	19.5	8.0
	↑Tr	32.4	28.7	18.3	18.1	8.5
W_m(7.2)/AF	400	76.4	28.7	16.0	18.0	6.6
	↑Tr	28.0	25.4	17.3	17.4	6.7
W_a(1.4)/KF	400	8.6	6.4	6.5	5.7	0.3
	↑Tr	3.8	4.1	3.4	3.8	0.8
W_a(3.0)/KF	400	22.4	17.8	14.9	12.7	1.0
	↑Tr	7.6	8.5	5.5	6.5	1.7
W_m(3.0)/KF	400	19.5	13.0	13.1	9.8	0.7
	↑Tr	4.4	4.4	2.4	3.0	1.7
W_m(7.3)/KF	400	14.4	6.3	7.9	3.9	0.7
	↑Tr	2.4	2.5	1.2	1.6	2.0

[a] ↑Tr: experiment increasing temperature, data at 400°C; n.a.: non available.

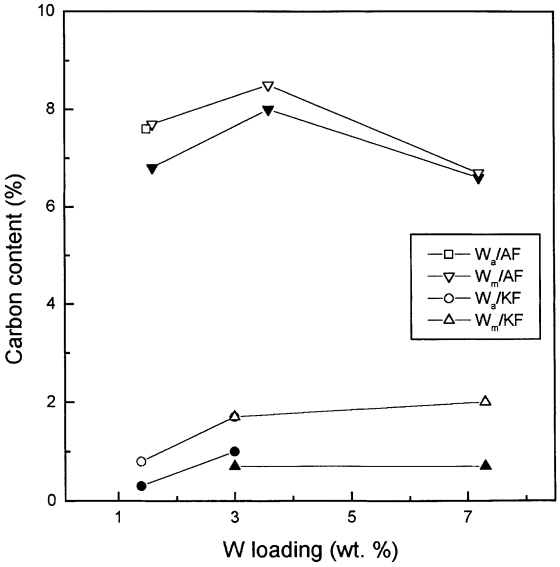

Fig. 3. Carbonaceous deposit after reaction at 400°C as a function of the tungsten loading on AF and KF. Starting the 1-butene feed with the bed either at 400°C (filled symbol) or at 200°C and then increasing temperature up to 400°C (open symbol).

with results previously reported [12,17]. Between 0.1 and 2.0%, the carbonaceous deposit on KF with and without tungsten is significantly lower. For each sample, the carbon content corresponding to the 1-butene fed with the bed at 400°C is slightly lower than the one obtained when the feed starts over the bed at a low temperature and then increasing it. This may be associated to the longer TOS resulting for these latter cases; the 1-butene stream is fed during the temperature increment, and then for 180 min at 400°C. Nevertheless, the difference does not modify the previous analysis, the carbonaceous deposit formed on W/KF being significantly lower than on W/AF, as shown in Fig. 3.

Fig. 4A and B present TPO profiles of different samples. W/AF profiles display two well-defined combustion peaks (centered at about 330 and 650°C, respectively), the high temperature one being larger. A shoulder at the beginning of the high-temperature combustion peak and/or a small peak at about 140°C appear on some samples. W/KF profiles show three well-defined combustion peaks: the smallest one centered at about 120°C, the main one centered at about 320–330°C, and the last peak above 500°C (its maximum shifts to a higher temperature by increasing the tungsten loading). These results indicate that the carbonaceous deposit formed on W/AF and W/KF has distinctive characteristic, related mainly to the different size of each combustion peak. Moreover, a minimum carbon content remains on W/KF at 600°C and all deposit is practically burnt out at 700°C, while a residual deposit still remains on W/AF above 700°C. It can play an important role when selecting regeneration conditions.

Before and after the butene skeletal isomerization, DRIFTS measurements on samples containing different tungsten loading were made. Table 2 presents bands of representative samples and their assignments. Bands above 3200 cm^{-1}, assigned to OH, are qualitatively similar for the only calcined W/AF and W/KF samples; the 3750 cm^{-1} centered band is practically the same and the other ones have lower intensity for W/KF. After reaction, the intensity of bands

Table 2
Bands (wavenumber values in cm^{-1}) observed in the 720–4000 cm^{-1} region of IR spectra on different samples and their assignments[a]

W/AF[b]	W_a(1.5)/AF	W_m(3.6)/AF	W_m(7.2)/AF	W_a(1.4)/KF	W_a(3.0)/KF	W_m(7.3)/KF	Assignment	Reference
	750 w	750 w	750 w				740–760: mono-substituted aromatics	[23]
790 s	800 m	800 m	800 w	820 m	795 m	795 m	790–840: CH deformation in alkenes	[23]
1020 s								
	1035 w	1035 w	1035 vw	1035 vw	1035 m	1035 w	1036/1045: $\upsilon CC/CH_3$ linear butene/i-$C_4^=$ bond π	[24]
	1140 w	1135 w	1135 vw	1130 vw	1130 w	1130 w	1110: linear butenes	[24]
1225 vs								
	1240 s	1240 s	1240 s	1245 s	1240 s	1240 s	1240: wagging CH_2 long chain paraffins	[23]
	1340 vw		1330 vw	1335 vw		1335 vw	1336: wagging $CH_2/iC_4^=$ dimeric	[25]
	1385 vw	1385 vw	1385 vw				1385: aromatics–polyaromatics/δ_s CH_3	[26]
				1390 vw	1390 w	1390 w	1390: olefinic species	[26]
	1425 vw	1430 vw		1425 vw		1420 w	1420/1430: linear butenes/δ $=CH_2$ vinyl	[24,25]
	1460 vw	1460 vw	1450 vw	1470 vw	1470 vw	1460 vw	1450/1463: arom.skeletal ring breathing/δ CH_3	[23,25]
	1520 m-s	1520 m-s	1520 m	1512 vw	1512 vw	1512 w	1513/1524: γ C=C aromatics	[13]
	1630 w	1627 w	1627 vw	1628 m	1628 m	1628 m	1630/1625: i-$C_4^=$ bond π/olefinic species	[25,27]
1640 m								
	2890 vw	2890 vw	2890 vw	2890 vw	2890 vw	2880 vw	2865–2925: saturated CH stretching	[27]
	2960 w	2960 w	2960 w	2960 vw	2960 vw	2960 vw	2960: saturated CH/polyolefins + aromatic	[26,27]
		2987 vw	2990 vw	2990 w	2990 w	2990 w	2970/2990: saturated CH/stretching CH/olefinics species	[26,27]
3250 w	3250 w	3250 w	3250 w	3250 vw	3250 vw	3250 vw	3200/3400: OH stretching, intermolecular, polymeric	[23]
3500 w	3500 vw	3500 vw	3500 vw	3500 vw	3500 vw	3500 vw		
3640 m	3640 m	3640 m	3640 w	3640 m	3640 m	3640 m	3609/3640: OH associated to Si/Al ions/OH in supercage	[28,29]
3750 vw	3750 vw	3750 vw	3750 vw	3750 vw	3750 vw	3750 vw	3742/3740: OH of terminal silanol/external sites	[28,29]

[a] vs: very strong; s: strong; m: medium; w: weak; vw: very weak.
[b] Only calcined sample.

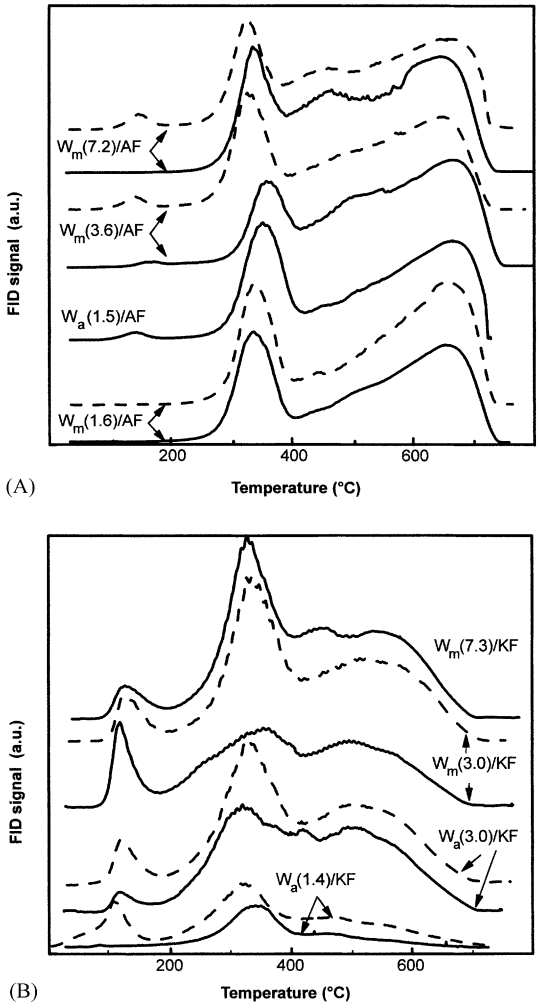

Fig. 4. TPO profiles of different samples. (A): W/AF; (B):W/KF. Starting the 1-butene feed with the bed either at 400°C (dashed line) or at 200°C and then increasing temperature up to 400°C (solid line).

centered at 3500 and 3640 cm^{-1} decreases while the small band at 3750 cm^{-1} remains practically constant. Characteristic bands of coke are detected on all samples, aliphatic and olefinic groups and aromatic rings are identified. Fig. 5 allows us to compare spectra of W/KF and W/AF representative samples, thus illustrating the extent of difference between the olefinic and aromatic coke components. Bands between 2865 and 2990 cm^{-1} and at 1240 cm^{-1} corresponding to aliphatic groups can be related to butene oligomers.

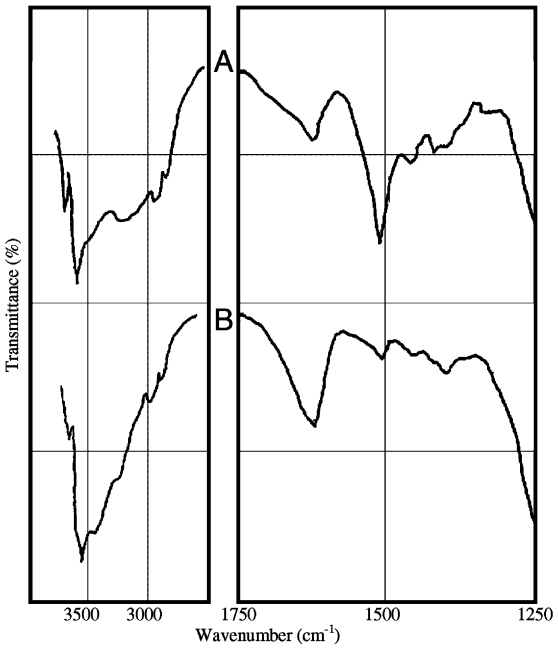

Fig. 5. DRIFTS spectra of representative samples after the 1-butene skeletal isomerization at 400°C. (A): W_m(3.6)/AF; (B): W_a(3.0)/KF.

4. Discussion

The improvement in isobutene selectivity with TOS, a characteristic behavior of ferrierite, has been related to the formation of carbonaceous deposit [10,12], to the type of acid site [28], and more recently to the acid site density [30] and to the space around the acid site [11]. Tungsten addition on AF produces a synergetic effect over the catalytic performance although it does not modify the behavior at short TOS. It suggests that the presence of tungsten does not produce a significant restriction to the reactant diffusion in the pores, as has been mentioned in order to explain the isobutene selectivity improvement [7,10]. KF is inactive in the linear butene skeletal isomerization while the tungsten addition promotes this reaction. The presence of tungsten species does not change significantly neither the acid strength distribution nor the total acidity. A similar qualitative behavior was reported for tungsten impregnated alumina: the tungsten species transform Lewis into Brønsted acid sites promoting the butene skeletal isomerization while alumina only isomerizes

the double-bond [31]. Nevertheless, alumina presents a black color at the end of the reaction while KF appears light brown. It can be explained considering the different acid strength distributions, alumina having strong acid sites [3,31] while KF only shows weak acid sites. Comparing KF with AF (with and without tungsten), the absence of high activity for W/KF at short TOS allows us to conclude that the strongest acid sites (high-temperature ammonia desorption peak) present in both AF and W/AF and absent in W/KF, are responsible for the high activity with a low isobutene selectivity. Then, the strongest acid sites would be involved as active sites in dimerization, oligomerization and cracking reactions. Recently, Wichterlová et al. [32] reported that Lewis acid sites on H-ferrierite enhance oligomerization and cracking reactions. These side-reactions have been suppressed by removing the non-selective acid sites using acid treatment [33,34].

The high activity of AF with and without tungsten at short TOS is also diminished by starting the reactant feed with the bed at 200°C and then increasing temperature up to 400°C [19]. This operating procedure changes the product distribution, decreasing the cracking activity and favoring the isobutene selectivity. It can be considered that the adsorption of linear butenes on the strongest acid sites takes place feeding the reactant with the bed at 200°C. The 1-butene irreversible adsorption on ferrierite below 350°C has been reported [35]. Other authors [36] also considered that butenes adsorbed at a low temperature oligomeryze to higher molecular weight compounds when temperature is raised, thus remaining adsorbed and reducing side-reactions. Then, considering that the strongest acid sites would be involved in the adsorption-oligomerization processes and knowing that cracking reactions demand higher acid strength sites than isomerization [37], we arrive at the same above conclusion, the strongest acid sites being responsible for the side-reactions.

By studying the carbonaceous deposit formed on different samples, qualitative and quantitative differences appear. The carbon content on AF with and without tungsten is 4–10 times larger than those corresponding to KF and W/KF, even starting the feed with the bed at 200°C for which case the high activity at short TOS is not reached. Polymerization reactions also demand higher acid strength than isomerization [37]. Consequently, as a first conclusion, the strong acid sites play an important role over the carbon content. TPO profiles display a significant difference in the size of the combustion peaks. The largest proportion of coke formed on AF and W/AF corresponds to the high-temperature combustion peak, it being difficult to eliminate and demanding severe conditions to be completely burnt out (i.e. 15 h at 660°C for AF [18]). These high combustion temperatures can be related to a more polymerized and less hydrogenated coke [38]. The largest proportion of the carbonaceous deposit on W/KF corresponds to the combustion peak appearing at moderate temperature (centered at about 320–330°C), and it is associated to a more hydrogen-rich coke [39]. For the latter samples, the low-temperature combustion peak can be related to adsorbed reactant molecules or to light oligomers [40]. The carbonaceous deposit corresponding to both low- and moderate-temperature combustion peaks can be eliminated by stripping using a helium stream [18]. It also suggests a hydrogen-rich coke, its removal demanding mild conditions. The coke structure can change during the TPO when temperature increases above the reaction one. Typically, the aromatic character of coke increases upon this treatment. This change in coke structure is more important as the acidity increases. The higher acidity of AF and W/AF is therefore responsible for the transformation of a larger amount of coke into aromatic coke during the TPO analysis. According to our results, it can be preliminarily concluded that the strength of acid sites present determines not only the carbonaceous deposit amount but also its degree of condensation.

According to DRIFTS results, characteristic bands assigned to paraffinic and olefinic species and to aromatic rings are present on all coked samples. It agrees with the previous TPO results, which show the same peaks although with different proportions. The weak band centered at about 750 cm^{-1} (assigned to mono-substituted aromatics) and the strong one at about 1520 cm^{-1} (assigned to γ-bond in C=C aromatics and associated to a coke with aromatic character [13]) allow us to consider that the largest proportion of carbonaceous deposit formed on AF with and without tungsten has an aromatic nature. Considering W/KF samples, the 750 cm^{-1} band does not appear, the 1520 cm^{-1} one is very weak, while bands at 1390 and 1420 cm^{-1} (assigned to linear butenes) and another one at about 1628 cm^{-1} (assigned to isobutene

π-bond and/or olefinic species [27]) increase. Coke formed on W/KF presents a larger olefinic nature. Other authors [10,41] reported the aromatic nature of the coke formed during the linear butene skeletal isomerization on ferrierite. Nevertheless, Xu et al. [10] assigned the 1622 cm^{-1} band to the stretching of butene double-bond while Guisnet et al. [41] employed a different technique in order to remove and characterize the coke.

The 3609 cm^{-1} band in the OH stretching range, which can shift to 3649 cm^{-1} after a steam treatment, is assigned to bridging OH groups known as the Brønsted acidic sites [33,42]. These acid sites are located in two positions showing a quite similar geometry and vibrating in large cavities; then, their infrared vibration frequency should be similar [43]. Measurement of both Brønsted acid sites has been recently reported [44]. According to our results, the 3609 cm^{-1} band decreases in all coked samples. It agrees with results previously reported [13,32], though the complete disappearance of that band by coke deposition has also been reported [45]. The carbonaceous deposit poisons acid sites, blocks channels and modifies the space around the sites improving the isobutene selectivity [10]. This improvement was verified by modifying the inner pores of ferrierite with a small weight loading of coke [12]. We also reported that a small amount of coke remaining on regenerated ferrierite samples improves the catalytic behavior compared to the fresh material [18]. Modeling studies were performed to characterize butene interactions with the Brønsted acid sites on ferrierite. A covalent alkoxide structure between the 1-butene and the acidic OH has been reported [46], although this type of reaction intermediates has little effect on the activation energies when hydrocarbon conversion on zeolites takes place [47]. The 1-butene adsorption on ferrierite mainly occurs in the channel intersection [36]. Recently, Wichterlová et al. [32] reported that hydroxyls located in large channels are accessible to isobutene molecules, while OH groups in eight-member ring channels are not. Coke deposition blocks channels increasing spatial constraints inside the pores and favoring the isobutene selectivity [10,30]. It has been employed to consider that the pore structure of ferrierite rather than its acidity plays an important role in achieving a high selectivity [7]. By studying the addition of metallic ions on SAPO-11, the isobutene selectivity improvement is related to the higher channel tortuosity by the metal ion substitution [48]. Comparing to ferrierite, the better catalytic performance of CoAlPO-11 is attributed to its monodimensional elliptic channels [49]. Nevertheless, the acidity characterization of cations containing catalysts shows only one desorption peak and the acidity of CoAlPO-11 was not measured, while the NH_3-TPD profile corresponding to ferrierite displays two desorption peaks [10,12]. Finally, deactivation has a strong influence over the acid sites concentration, and therefore affects the concentration of adsorbed butene molecules, thus favoring different reactions. A high molecules concentration accelerates the multimolecular oligomerization while a low concentration induces the monomolecular reaction thus resulting in a high isobutene selectivity [30]. Consequently, the study of deactivation cannot be separated from the acidity analysis. The primary analysis should be centered into the acidity because it affects both selectivity and coke formation while the carbonaceous deposit influences the selectivity by changing the state of the fresh material. According to our results, the acid strength distribution plays an important role when stability and deactivation of catalysts are studied.

5. Conclusions

After tungsten addition on both potassium and ammonium ferrierite samples, neither the acid strength distribution nor the total acidity corresponding to the unpromoted materials change significantly. The strongest acid sites (high-temperature ammonia desorption peak) present in both AF and W/AF and absent in W/KF, are involved as active sites in dimerization, oligomerization and cracking reactions, being responsible for the side-reactions.

Deactivation of tungsten promoted ferrierites shows qualitative and quantitative differences. AF and W/AF reach similar carbon contents, being larger than the ones obtained on KF and W/KF. In all cases, the carbonaceous deposit shows both olefinic and aromatic species, the proportion depending on the samples. Coke on W/KF shows mainly an olefinic nature, while the deposit formed on W/AF has a more aromatic character. For the latter samples, the complete coke removal needs higher temperatures. The strength of

acid sites present on the samples determines not only the carbonaceous deposit amount but also its degree of condensation.

The low isobutene selectivity at short TOS showed by AF and W/AF is avoided by starting the 1-butene feed with the catalytic bed at 200°C and then increasing temperature up to 400°C. It can be considered that a strong adsorption of reactant molecules takes place at low temperatures, deactivating the strongest acid sites. Consequently, the acid strength distribution plays an important role when stability and deactivation are studied.

Acknowledgements

The authors are indebted to JICA (Japan International Cooperation Agency) for the donation to CENACA (National Catalysis Center) of equipments for catalyst characterization and to TOSOH for the provision of ferrierite sample. The financial assistance of CAI + D (UNL) and CONICET is also acknowledged. The authors acknowledge E. Grimaldi for her help in editing the English manuscript.

References

[1] B.G. Baker, N.J. Clark, in: A. Crucq, A. Frennet (Eds.), Catalysis and Automotive Pollution Control, Studies in Surface Science and Catalysis, Vol. 30, Elsevier, Amsterdam, 1987, p. 483.
[2] A.C. Butler, C.P. Nicolaides, Catal. Today 18 (1993) 443.
[3] V. Benitez, C.A. Querini, N.S. Fígoli, R.A. Comelli, Appl. Catal. 178 (2) (1999) 205.
[4] M.W. Simon, W.Q. Xu, S.L. Suib, C.L. O'Young, Microporous Mater. 2 (1994) 477.
[5] L.H. Gielgens, I.H.E. Veenstra, V. Ponec, M.J. Haanepen, J.H.C. van Hooff, Catal. Lett. 32 (1995) 195.
[6] G. Seo, H.S. Jeong, S.B. Hong, Y.S. Uh, Catal. Lett. 36 (1996) 249.
[7] P. Mériaudeau, A. Vu Tuan, N. Le Hung, G. Szabo, Catal. Lett. 47 (1997) 71.
[8] J. Houzvicka, S. Hansildaar, V. Ponec, J. Catal. 167 (1997) 273.
[9] W.M. Meier, D.H. Olson, in: Atlas of Zeolite Structure Types, 3rd Edition., Butterworths–Heinemann, London, 1992, p. 98.
[10] W.Q. Xu, Y.G. Yin, S.L. Suib, C.L. O'Young, J. Phys. Chem. 99 (1995) 758.
[11] P. Mériaudeau, V.A. Tuan, L.N. Hung, C. Naccache, G. Szabo, J. Catal. 171 (1997) 329.
[12] G. Seo, H.S. Jeong, D.L. Jang, D.L. Cho, S.B. Hong, Catal. Lett. 41 (1996) 189.
[13] P. Andy, N.S. Gnep, M. Guisnet, E. Benazzi, C. Travers, J. Catal. 173 (1998) 322.
[14] J. Houzvicka, V. Ponec, Ind. Eng. Chem. Res. 37 (1998) 303.
[15] M. Guisnet, P. Magnoux, Catal. Today 36 (1997) 477.
[16] R.A. Comelli, Z.R. Finelli, N.S. Fígoli, C.A. Querini, in: C.H. Bartholomew, G.A. Fuentes (Eds.), Catalyst Deactivation 1997, Studies in Surface Science and Catalysis, Vol. 111, Elsevier, Amsterdam, 1997, p. 139.
[17] M. Guisnet, P. Andy, Y. Boucheffa, N.S. Gnep, C. Travers, E. Benazzi, Catal. Lett. 50 (1998) 159.
[18] Z.R. Finelli, C.A. Querini, N.S. Fígoli, R.A. Comelli, Appl. Catal. A 187 (1999) 115.
[19] Z.R. Finelli, N.S. Fígoli, R.A. Comelli, Catal. Lett. 51 (1998) 223.
[20] S.C. Fung, C.A. Querini, J. Catal. 138 (1992) 240.
[21] J.S. Lee, M.H. Yeom, D.S. Park, J. Catal. 126 (1990) 361.
[22] C.L. O'Young, W.Q. Xu, M. Simon, S.L. Suib, in: J. Weitkamp, H.G. Karge, H. Pfeifer, W. Hölderich (Eds.), Zeolites and Related Microporous Materials: State of the Art 1994, Studies in Surface Science and Catalysis, Vol. 84, Elsevier, Amsterdam,1994, p. 1671.
[23] L.J. Bellamy, The Infra-red Spectra of Complex Molecules, 3rd Edition, Chapman & Hall, London, 1975.
[24] N. Sheppard, C. de la Cruz, in: D.D. Eley, W.O. Haag, B. Gates (Eds.), Vibrational Spectra of Hydrocarbons Adsorbed on Metals, Advances in Catalysis, Vol. 41, Academic Press, London, 1996, p. 1.
[25] S. Meijers, L.H. Gielgens, V. Ponec, J. Catal. 156 (1995) 147.
[26] C. Li, P.C. Stair, Catal. Today 33 (1997) 353.
[27] M. Trombetta, G. Busca, S. Rossini, V. Piccoli, U. Cornaro, J. Catal. 168 (1997) 349.
[28] W.Q. Xu, Y.G. Yin, S.L. Suib, J.C. Edwards, C.L. O'Young, J. Phys. Chem. 99 (1995) 9443.
[29] D. Eisenbach, E. Gallei, J. Catal. 56 (1979) 377.
[30] G. Seo, N.H. Kim, Y.H. Lee, J.H. Kim, Catal. Lett. 57 (1999) 209.
[31] S.L. Soled, G.B. McVicker, L.L. Murrell, L.G. Sherman, N.C. Dispenziere Jr., S.L. Hsu, D. Waldman, J. Catal. 111 (1998) 286.
[32] B. Wichterlová, N. Zilkova, E. Uvarova, J. Cejka, P. Sarv, C. Paganini, J.A. Lercher, Appl. Catal. A 182 (1999) 297.
[33] W.Q. Xu, Y.G. Yin, S.L. Suib, J.C. Edwards, C.L. O'Young, J. Catal. 163 (1996) 232.
[34] B.S. Kwak, J. Sung, Catal. Lett. 53 (1998) 125.
[35] K.P. de Jong, H.H. Mooiweer, J.G. Buglass, P.K. Maarsen, in: C.H. Bartholomew, G.A. Fuentes (Eds.), Catalyst Deactivation 1997, Studies in Surface Science and Catalysis, Vol. 111, Elsevier, Amsterdam, 1997, p. 127.
[36] G. Seo, S.H. Park, J.H. Kim, Catal. Today 44 (1998) 215.
[37] S.H. Baeck, K.M. Lee, W.Y. Lee, Catal. Lett. 52 (1998) 221.
[38] J. Barbier, E. Churín, P. Marecot, J.C. Menezo, Appl. Catal. 36 (1988) 277.
[39] C.A. Querini, Catal. Today 62 (2000) 135.
[40] C.A. Querini, E. Roa, Appl. Catal. A 163 (1997) 199.
[41] M. Guisnet, P. Andy, N.S. Gnep, C. Travers, E. Benazzi, in: H. Chon, S.K. Ihm, Y.S. Uh (Eds.), Progress in Zeolite and Microporous Materials, Studies in Surface Science and Catalysis, Vol. 105, Elsevier, Amsterdam, 1997, p. 1365.

[42] B. Lee, J.N. Kondo, K. Domen, F. Wakabayashi, J. Mol. Catal. A 137 (1999) 269.
[43] A. Martucci, A. Alberti, G. Cruciani, P. Radaelli, P. Ciambelli, M. Rapacciulo, Microporous Mesoporous Mater. 30 (1999) 95.
[44] A.G. Palkhiwala, R.J. Gorte, Catal. Lett. 57 (1999) 19.
[45] J. Datka, in: B. Imelik, C. Naccache, Y. Ben Taarit, J.C. Vedrine, G. Coudurier, H. Praliaud (Eds.), Studies in Surface Science and Catalysis, Vol. 5, Elsevier, Amsterdam, 1980, p. 121.
[46] R. Millini, S. Rossini, Progress in Zeolite and Microporous Materials, in: H. Chon, S.-K. Ihm, Y.S. Uh (Eds.), Studies in Surface Science and Catalysis, Vol. 105, Elsevier, Amsterdam, 1997, p. 1389.
[47] A.M. Rigby, G.J. Kramer, R.A. van Santen, J. Catal. 170 (1997) 1.
[48] S.M. Yang, J.Y. Lin, D.H. Guo, S.G. Liaw, Appl. Catal. A 181 (1999) 113.
[49] J. Cejka, B. Wichterlová, P. Sarv, Appl. Catal. A 179 (1999) 217.